Two modes resonant combined motion for insect wings kinematics reproduction and lift generation

Damien Faux, Eric Cattan, Olivier Thomas, Sébastien Grondel

Two modes resonant combined motion for insect wings kinematics reproduction and lift generation

D. Faux[1], O. Thomas[2], E. Cattan[1] and S. Grondel[1]

[1] *Univ. Valenciennes, CNRS, Univ. Lille, YNCREA, Centrale Lille, UMR 8520 - IEMN, DOAE F-59313 Valenciennes, France*
[2] *Arts et Metiers ParisTech, LSIS - UMR 7296 - 8 boulevard Louis XIV, 59046 Lille, France*

Abstract – This paper presents an original concept using a two resonant vibration modes combined motion to reproduce insect wings kinematics and generate lift. The key issue is to design the geometry and the elastic characteristics of artificial wings such that a combination of flapping and twisting motions in a quadrature phase shift could be obtained. This qualitatively implies to bring the frequencies of the two resonant modes closer. For this purpose, a polymeric prototype was micromachined with a wingspan of 3 cm, flexible wings and a single actuator. An optimal wings configuration was determined with a modeling and validated through experimental modal analyses to verify the proximity of the two modes frequencies. A dedicated lift force measurement bench was developed and used to demonstrate a lift force equivalent to the prototype weight. Finally, at the maximum lift frequency, high-speed camera measurements confirmed a kinematics of the flexible wings with flapping and twisting motions in phase quadrature as expected.

Introduction. – Among flying species observed in nature, insects certainly demonstrate the most impressive capacities in terms of hovering, backward flight or sudden acceleration, and their diversity offers multiple solutions for bio-inspired systems. The understanding of insect flight has improved considerably and it is well known that lift results from a wide array of unconventional aerodynamic mechanisms [1] as well as specific kinematics induced by the flexible characteristics of the wings [2]. More precisely, as illustrated in fig. 1 through the generic periodic motion of the wing cross section in the chord direction, insect wings kinematics relies on the combination of four basic motions: the downstroke, the supination, the upstroke and the pronation [3,4]. In the case of flexible wings, the up and downstrokes involve a flapping motion, corresponding to a change of stroke angle θ, whereas supination and pronation result in a twisting motion, a change in angle of attack φ, in quadrature with the previous one. This phase quadrature, *i.e.*, when the amplitude is maximal for one motion it is null for the other, produces aerodynamic forces and contributes to generate lift.

As already mentioned, a key element of insect flight is the flexibility of the wings structure that often changes

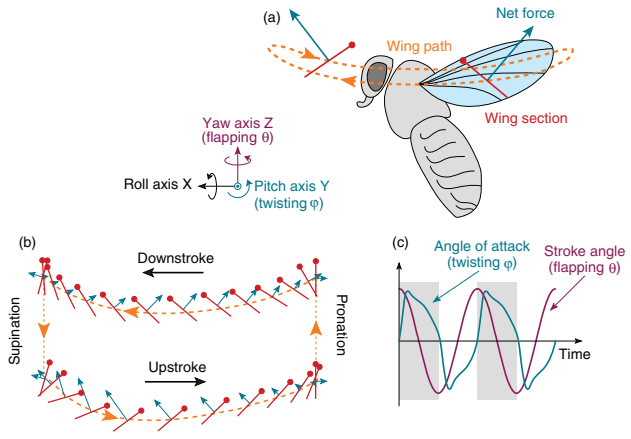

Fig. 1: (Colour online) Insect wings motion: (a) wing path described by looking at a particular section of the wing (in red) with the dots representing the leading edge; (b) tracking of this wing section during up and downstrokes demonstrating their translational motion and showing slope reversal due to pronation and supination interpreted as rotational motion; (c) trend in evolution of stroke angle θ (flapping) and angle of attack φ (twisting) in quadrature over time [5,6].

shape dynamically during flight [7], but its exact role in aerodynamic performance remains unclear and controversial. Several studies [2,8,9] have provided direct evidence that flexible wings able to produce camber generate higher peak lift forces than rigid wings [10,11], but recent simulation work [12] has demonstrated that at low and medium angles of attack, aerodynamic performance decreases with greater flexibility. Furthermore, the employment of resonant mechanisms has also been the subject of much discussion. Indeed some studies highlight the use of the natural frequency of wings [13,14] that yields excellent performance with low power consumption, and others demonstrate on the contrary that insects have a wing beat that is different from the resonant frequencies of the wings [7,15] as the resonant mechanism depends on other body parts such as the thorax [16].

The leading idea of this work is the design of a prototype with fully flexible wings able to generate lift, using the resonance properties of the wings to obtain a large amplitude motion. Since a non-synchronous resonant kinematics is necessary —a flapping and a twisting motion in quadrature— at least two vibration modes have to be coupled, or at least simultaneously actuated. Historically, the concept of mode coupling has already been used in the fields of optics, photonics, and chemistry [17,18], as well in micro-electro-mechanical systems (MEMS) to increase the sensitivity of vibrational gyroscopes [19,20]. In music, instrument structures are also designed to tune mode frequencies non-linearly to produce complex sounds [21–23]. However, as far as we know, mechanical vibration modes are generally shifted away from working frequencies to avoid destructive interactions with a system and are rarely used to perform a specific mechanism.

The purpose of this paper is to prove that it is possible to design a fully flexible wing structure so that a coupled motion of two vibration modes (flapping and twisting) in phase quadrature —close to an insect-like wings kinematics able to generate lift— is naturally obtained with a single actuator acting at a single frequency, without trying to mimick real insects wings geometries and actuation.

Proposed concept. – In this study, we consider a fully flexible wing (fig. 2) whose kinematics is defined by the combination of two elementary motions: a flapping motion, described by a rotation of stroke angle θ around the Z-axis, and a twisting motion, described by a rotation of angle of attack φ around the Y-axis (refer to fig. 1 for the axis definition).

In general, artificial wings of micro and nano air vehicles consist of an articulated rigid leading edge attached to the thorax and a flexible membrane [24,25]. To produce an appropriate wing slope and lift off [26], the most common mechanism is to impose a large flapping motion on the rigid leading edge and to exploit the passive twisting of the wings. In this case, the wing is equivalent to a single degree of freedom system in twisting with the displacement of the leading edge during a flapping imposed.

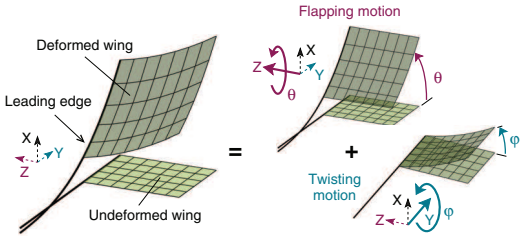

Fig. 2: (Colour online) A flexible wing whose instantaneous shape is described by the combination of a flapping and a twisting motion.

The new concept proposed here is to design a flexible wing such that the leading edge displacement and the twisting are both induced by the dynamic resonant behavior of the structure, with the proper combination to produce phase quadrature. To obtain such specific kinematics, the proposed solution is 1) to consider two natural vibration modes of which the deformed shapes are close to a flapping motion for the first one and close to a twisting motion for the second one, 2) to design the geometry and the elastic characteristics of the wings structure so that their natural frequencies are close to each other and 3) to simultaneously actuate the two modes with a single frequency in phase quadrature.

To illustrate this concept, let us consider a reduced-order dynamical model of the flexible wings, truncated to only two natural modes. The displacement of a point x of the wings is written as a function of space and time:

$$u(x,t) = \Phi_1(x)q_1(t) + \Phi_2(x)q_2(t) \qquad (1)$$

with $q_1(t)$ and $q_2(t)$ being the modal coordinates and $\Phi_1(x)$ and $\Phi_2(x)$ the modal shapes of the two retained modes (flapping and twisting, respectively). These two mode shapes are illustrated in fig. 3(a), (b): the flapping mode shape Φ_1 corresponds to a motion with a preponderant θ rotation around the Z-axis, whereas the twisting mode shape Φ_2 results in a preponderant φ rotation around the Y-axis. Notice that the mode shapes of fig. 3(a), (b) do not correspond to pure flapping (θ) and twisting (φ) motions (an example of pure flapping and twisting motions is shown in fig. 2) since they are the ones of the prototype of fig. 4, thus resulting from its structural vibratory properties.

According to classical vibration theory [27], the two modal coordinates $q_1(t)$ and $q_2(t)$ satisfy the following differential equations:

$$\ddot{q}_i(t) + 2\xi_i\omega_i\dot{q}_i(t) + \omega_i^2 q_i(t) = F_i \cos\Omega t, \quad i = 1,2, \qquad (2)$$

where ξ_1 and ξ_2 are the damping factors of each mode, ω_1 and ω_2 their natural frequencies, F_1, F_2 the modal forcing terms and Ω the harmonic excitation frequency. These modal coordinates can be written $q_1(t) = a_1\cos(\Omega t + \alpha_1)$ and $q_2(t) = a_2\cos(\Omega t + \alpha_2)$ in the steady state. If $\xi_i < \sqrt{2}$, the response is resonant as shown in fig. 3(c), (d) ((1) for

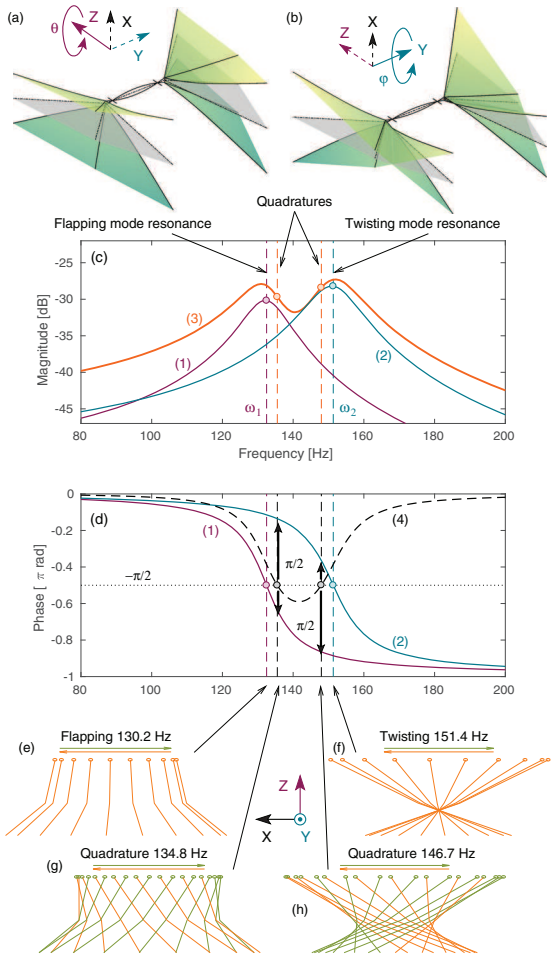

Fig. 3: (Colour online) Theoretical mode shapes of the prototype: (a) flapping; (b) twisting. Amplitude and phase of the theoretical frequency responses of the prototype: (c) amplitude of (1) flapping and (2) twisting modal coordinates; (3) amplitude of their combination; (d) flapping (1) and twisting (2) phases and their difference (4). Wing tip motion tracking seen from the Y-side (in the (X, Z)-plane): (e) flapping resonance, (f) twisting resonance, ((g), (h)) quadrature motions.

the flapping mode and (2) for the twisting mode). The frequency response of the wings is also shown (line (3)) and results from the modal combination of eq. (1).

Amplitudes a_1 and a_2 are maximum for $\Omega \simeq \omega_1, \omega_2$, where the phases α_1, α_2 cross the $\pi/2$ value. As shown in fig. 3(d), between the resonance frequencies, there are two other frequencies for which the phase difference is $\alpha_2 - \alpha_1 = \pi/2$ and corresponds to kinematics with the flapping and twisting motion in quadrature. To illustrate these particular kinematics, wing tip motion tracking, seen from the side, is shown in fig. 3(e)–(h). For an excitation frequency close to the two flapping and twisting resonances ($\Omega \simeq \omega_1, \omega_2$), the wings motion is synchronous and corresponds to one of the oscillatory mode shapes. As explained in the introduction, a lift is generated if a phase shift between the leading edge and the trailing edge of the wings occurs. Consequently, for those synchronous

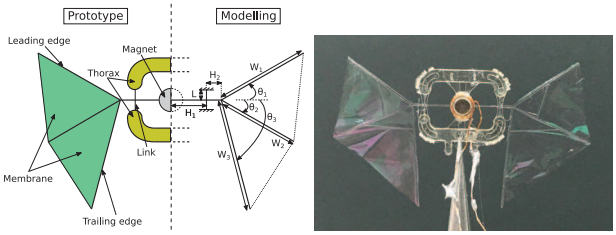

Fig. 4: (Colour online) Prototype with SU-8 skeleton, Parylene C wings and electromagnetic actuator with a total mass of 22 mg and 22 mm wingspan.

motions, no lift is theoretically generated. Conversely, at the two quadrature frequencies (fig. 3(g), (h)) the flapping and twisting mode shapes are both activated in quadrature, in a motion very close to the insect wings kinematics (fig. 1), since the maximum angle of attack occurs when the wing is halfway of the upstroke and the downstroke, with slope reversal at the end of each stroke.

Consequently, the proposed concept has two remarkable effects. First, due to an appropriate combination of the flapping and twisting motion of the artificial wings, a kinematic similar to insects ones can be created. Second, since the two quadrature actuation frequencies are close to the flapping and twisting resonances, a large amplitude of the wings, suitable to maximize the lift force, could be obtained.

Prototype design. – The prototype was fabricated with dedicated MEMS technologies to allow highly accurate design tolerance. It is composed of a 3D skeleton made from multiple layers of SU-8 photoresist, with thicknesses ranging between 40 μm and 150 μm (fig. 4). The wings membranes, composed of a 400 nm thick film of Parylene C, were deposited on the skeleton veins, resulting in wings 22 mm in length. All the details can be found in [28]. The obtained fully polymeric wings structure is considered as equivalent to that of natural insect wings [29–31].

The wings are driven simultaneously by a single electromagnetic actuator placed at the middle of the thorax and actuated by a sinusoidal current. It comprises a magnet stuck in the middle of the thorax which is slipped into a copper coil fixed to the thorax, as presented in fig. 4. A cylindrical neodymium-iron-boron magnet (Ni-N48) with a thickness of 0.5 mm, a diameter of 1.5 mm, and a mass of 6 mg was selected. The coil was made in-house using a 80 μm diameter enameled copper wire, the number of turns was 20. This electromagnetic actuator has the advantage of being easy to manufacture and integrate into our prototype, having a simple geometry, fast response speed, high bandwidth, and more particularly, the possibility of tuning a wide range of frequencies. The total weight of the prototype is 22 mg, which places it in the insects dimensions range.

The flexible structure of the wings was modeled using an assembly of continuous Euler-Bernoulli beam models,

deforming in vacuum and built in homogeneous and isotropic SU-8 polymer with Young's modulus of 2 GPa. The structural effect of the wings membranes was neglected, as their thickness is very small compared to the veins. These assumptions are justified since our primary goal was to design the wings geometry such that the natural frequencies of the flapping and twisting vibration modes were close. To this end, an optimization of the geometrical parameters $(\theta_i, W_i, H_i \ldots)$ of the wings vein geometry of fig. 4, based on a numerical modal analysis [32], was performed. The main constraints were to bring the frequencies of the two natural modes as close as possible to each other and lying between 100 Hz and 200 Hz. The geometry of the thorax was imposed. For more details about the model and the optimization, the interested reader can refer to [33].

According to the optimization study, an optimal configuration of the wings vein structure was found, as illustrated in fig. 4. Its frequency response is shown in fig. 3, with damping ratios $\xi_1 = \xi_2 = 5\%$ chosen in eqs. (2) to fit the experiments. The viscous damping included here is used to take into account the damping effect of the aeroelastic forces. Even though multiple solutions exist, the one proposed here appears to be satisfactory since the two combined modes are only 20 Hz apart with the flapping mode occurring at 130.2 Hz and the twisting mode at 151.4 Hz for the wings designed. This now means that quadrature combination of these modes is possible just by tuning the excitation frequency, with two solutions, at 134.8 Hz and at 146.7 Hz, very close to the flapping and twisting resonances, thus resulting in a relatively large amplitude of wings motion.

Experimental setups. – In order to estimate both the kinematics and the lift force generated by the prototype during wings actuation, a specific test bench was developed. It comprises a brass cantilever beam to which the prototype was glued, the goal being to correlate the cantilever displacement with the prototype aerodynamic force.

To evaluate the kinematics, a Polytec PSV400 scanning laser vibrometer was used to measure the velocity at several points on the skeleton of the prototype during sine sweep input excitation for small flapping amplitudes. Precisely, the frequency spectrum of the velocity signal was divided by that of the input electric current in the coil to obtain the Frequency Response Function (FRF) of the corresponding point. As the laser vibrometer is not able to measure large amplitude motions of the wings, a high-speed camera (Phantom V7.4 from Vision) was employed to record the wings kinematics for high flapping amplitudes.

The laser vibrometer was also used to measure the passive response of the brass beam to identify the value of its lowest resonance frequency. It was then verified that it was greater than twice those of the prototype flapping and twisting resonance frequencies, which lie between 120 Hz and 220 Hz. This condition was necessary to ensure that the cantilever displacement could be used to determine the lift force generated by a simple proportionality relation independent of the actuation frequency.

The linear relationship between the force applied to the cantilever tip and its jib was evaluated at 180 μN/μm using both an FT-S1000 microforce sensing probe and an FT-1000 mechanical probe from Femto-Tools. The lift force was then obtained during wings prototype actuation by measuring the displacement of the cantilever using a laser (LK-G32 Keyence) that can measure displacements in the order of 0.1 μm, so a minimum force of approximately 18 μN could be measured.

Results and discussion. – The experimental setup described previously is used to test the performance of several prototypes (a batch of 8) of the optimal configuration seen on fig. 4. They all share the same qualitative and quantitative behaviour, which is described hereafter. The quantitative experimental results are those of one of the prototypes.

First, the FRFs at several points on a prototype skeleton were measured using the PSV400 scanning laser vibrometer. These values were then used to reconstruct the deflection shape of the prototype at several actuation frequencies. Two FRFs (one at the magnet and one at the leading edge of the left wing) are depicted in fig. 5(c) and show two resonances at 140 Hz and 195 Hz. The corresponding experimental deflection shape animations[1] were found synchronous (all points reach the zero position and their extremum at the same time), proving that they correspond to the deformed shape of the modes. A frozen image of these two deformed shapes is shown in fig. 5(a), (b), clearly assessing that they are associated with the flapping and twisting modes. Out of these two resonances, the motion of the wings is no more synchronous and for some frequencies, motions with the leading and trailing edge in phase quadrature were observed[2].

These experimental results are impressively close to those obtained in simulation. First, the experimental mode shapes are similar to the ones predicted (compare fig. 5(a), (b) and fig. 3(a), (b)). Then, a minimal difference in frequency of 60 Hz was successfully obtained between the flapping and twisting modes, whereas the theoretical difference was smaller (about 20 Hz). However, it must be recalled that our modeling is used for pre-sizing our prototype. This discrepancy can then be explained by the aeroelastic effects neglected in the model, responsible for damping and added mass effects that change the resonance frequencies.

In a second step, using the proposed test bench, the lift force was measured in the steady state at several frequencies around the flapping and twisting resonance

[1] See the movies at 140 Hz and 195 Hz in the supplementary material: `Vibrometer140Hz.avi` and `Vibrometer195Hz.avi`.

[2] See the movie at 190.8 Hz in the supplementary material: `Vibrometer190Hz.avi`.

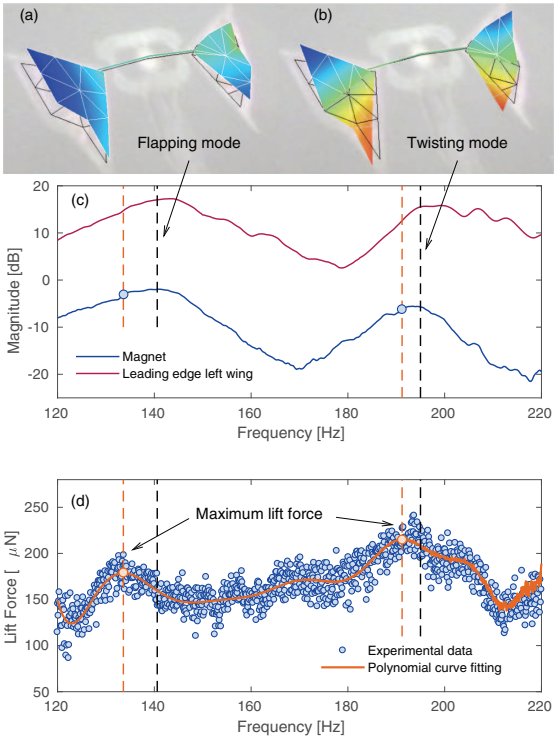

Fig. 5: (Colour online) Experimental deflection shapes at resonance: (a) flapping mode; (b) twisting mode. (c) FRF of the prototype taken at the magnet and leading edge left wing, zoomed over the frequency range of interest. (d) Average lift force over one period for several excitation frequencies. Polynomial curve fit.

frequencies. Figure 5(d) shows the lift force averaged out over a period of motion and a polynomial curve fit. Good precision was obtained for such levels of force since an uncertainty of approximately 10% was observed. Furthermore, two local maxima of the averaged lift force were observed near the flapping and twisting modes at 133.5 Hz and 190.8 Hz, respectively. By observing the motion of the wings by means of the high-speed camera, as illustrated in fig. 6 and[3], these two maximum values correspond to the expected wings kinematics with the leading and trailing edges in phase quadrature, similar to those predicted by the theory (fig. 3(d)). In fig. 6, angles of flapping and twisting ranges are approximately of 20°.

In fig. 5(c), one can observe that the low-frequency lift maximum is below the resonance of the flapping mode frequency instead of being above, as predicted by theory. This discrepancy can firstly be explained by non-linear effects. Indeed, the frequency responses given in fig. 5(c) are obtained for small (linear) flapping amplitudes (under 0.2 mm), with the laser vibrometer which is not able to measure large amplitude motions. On the contrary, the lift forces measurements provided in fig. 5(d) are processed at high flapping amplitudes (around 10 mm). Considering the non-linearities due to the aeroelastic effects and the

[3]See the high-speed camera movie in the supplementary material: `SpeedCam_190Hz.mov`.

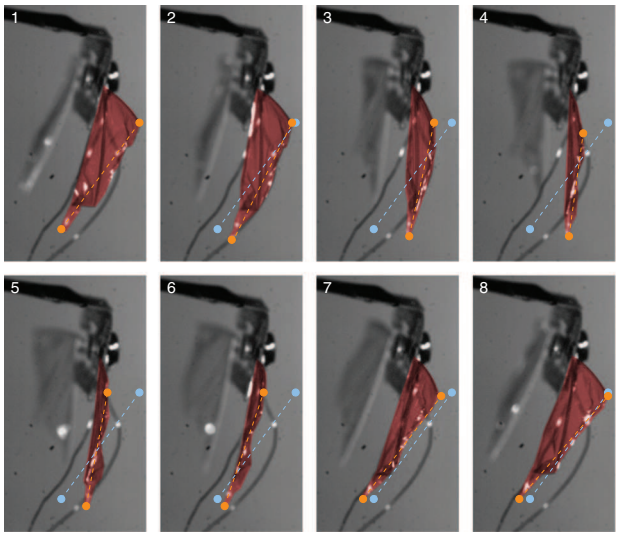

Fig. 6: (Colour online) Several frames captured using a high-speed camera at the second quadrature actuation frequency (190.8 Hz). Blue dashed line: initial chord position; orange dashed line: current chord position. Slope inversion occurs around frame 4.

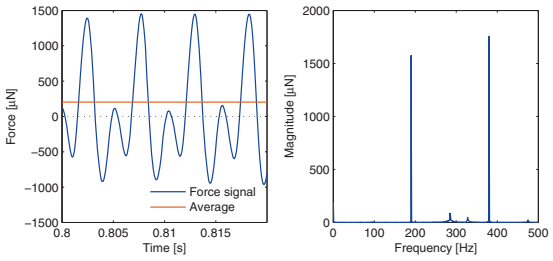

Fig. 7: (Colour online) Lift force *vs.* time at the second quadrature actuation frequency (190.8 Hz) and related frequency spectrum.

large amplitude motion of the wings structure (geometricals non-linearities), the modes resonance frequencies are probably slightly shifted at large amplitude (fig. 5(d)) with respect to the small amplitude (fig. 5(c)), which can explain these discrepancies. Secondly, the time necessary for the measurements of fig. 5(d) is very long (10 hours for the 1000 measurement points), which probably causes a structural fatigue of the prototype, also probably responsible of the frequency shift. The exact characterisation of these effects is beyond the scope of this article, devoted to the proof of concept of the quadrature kinematics of the wings, validated, as explained above, at the lift force maxima with the high-speed camera acquisitions.

In addition to this discussion, fig. 7 presents the instantaneous force measured as a function of time as well as the associated frequency spectrum for the second quadrature frequency. In addition to the continuous component, two frequency peaks can be distinguished: one at the actuation frequency of 190.8 Hz corresponding to the drag force, and the other at the second-harmonics frequency of

381.6 Hz associated with the lift force, as frequency doubling is related to slope variation during the strokes. As shown by [4,34], the averaged force obtained corresponds to the effective lift force.

Finally, at the high-frequency maxima, near the twisting mode, the lift force reaches 240 μN, a value sufficient to overcome the prototype weight, equivalent to 220 μN. The main goal of this study, which was to use a quadrature combination of two resonant modes to produce lift, was definitely achieved and validated. Future work must now focus not only on wings configuration but also on the actuation and transmission parts in order to increase the flapping amplitude and enable take off.

* * *

This work was supported by ANR-ASTRID CLEAR-Flight (ANR-13-ASTR-0012), RENATECH program, Direction Generale de l'Armement and Haut-de-France Region.

REFERENCES

[1] Srygley R. and Thomas A., *Nature*, **420** (2002) 660.
[2] Wootton R., *Adv. Odonatol.*, **5** (1991) 153.
[3] Wootton R., *Nature*, **400** (1999) 112.
[4] Dickinson M., *Science*, **284** (1999) 1954.
[5] Fry S. N., Sayaman R. and Dickinson M. H., *Science*, **300** (2003) 495.
[6] Seshadri P., Benedict M. and Chopra I., *Bioinspir. Biomim.*, **7** (2012) 036017.
[7] Chen J.-S., Chen J.-Y. and Chou Y.-F., *J. Sound Vibrat.*, **313** (2008) 643.
[8] Ennos A. R., *J. Exper. Biol.*, **140** (1988) 137.
[9] Ennos A. R., *J. Exper. Biol.*, **140** (1988) 161.
[10] Mountcastle A. and Daniel T. L., *Exper. Fluids*, **46** (2009) 873.
[11] Young J., Walker S., Bomphrey R., Taylor G. and Thomas A., *Science*, **325** (2009) 1549.
[12] Zhao L., Huang Q., Deng X. and Sane S., *J. R. Soc. Interface*, **7** (2010) 485.
[13] Michelin S. and Llewellyn Smith S., *Phys. Fluids*, **21** (2009) 071902.
[14] Masoud H. and Alexeev A., *Phys. Rev. E*, **81** (2010) 056304.
[15] Ha N., Truong Q., Goo N. and Park H., *Bioinspir. Biomim.*, **8** (2013) 046008.
[16] Hrncir M., Gravel A.-I., Schorkopf D., Schmidt V., Zucchi R. and Barth F., *J. Exp. Biol.*, **211** (2008) 678.
[17] McCutcheon M., Young J., Rieger G., Dalacu D., Frederick S., Poole P., Aers G. and Williams R., *Physics*, **2** (2006) 0601021.
[18] Misochko O. V., Rasi-Iba E. I., Sherman E. Y. and Timofeev V. B., *Phys. Rep.*, **6** (1990) 387.
[19] Zaman M., Sharma A. and Ayazi F., in *Proceedings of the 19th International Conference on Micro Electro Mechanical Systems* (IEEE) 2006, p. 66.
[20] Leland R., *IEEE Trans. Control Syst. Technol.*, **11** (2003) 242.
[21] Monteil M., Thomas O. and Touzé C., *Appl. Acoust.*, **89** (2015) 1.
[22] Rossing T. and Perrin R., *Appl. Acoust.*, **20** (1987) 41.
[23] Fletcher N., *Appl. Acoust.*, **39** (1993) 145.
[24] Wood R., *IEEE Trans. Robot.*, **24** (2008) 341.
[25] Raney D. and Slominski E., in *AIAA Guidance, Navigation, and Control Conference and Exhibit* (AIAA) 2003, article No. 5345.
[26] Ramananarivo S., Godoy-Diana R. and Thiria B., *Proc. Natl. Acad. Sci. U.S.A.*, **108** (2011) 5964.
[27] Géradin M. and Rixen D., *Mechanical Vibrations: Theory and Applications to Structural Dynamics* 3rd edition (J. Wiley & Sons) 2015.
[28] Bao X., Bontemps A., Grondel S. and Cattan E., *J. Micromech. Microeng.*, **21** (2011) 125020.
[29] Bontemps A., Vanneste T., Paquet J.-B., Dietsch T., Grondel S. and Cattan E., *Smart Mater. Struct.*, **22** (2013) 014008.
[30] Dargent T., Bao X., Grondel S., Brun G. L., Paquet J.-B., Soyer C. and Cattan E., *J. Micromech. Microeng.*, **19** (2009) 085028.
[31] Bao X., Dargent T., Grondel S., Paquet J. and Cattan E., *Microelectron. Eng.*, **88** (2011) 2218.
[32] Wittrick W. H. and Williams F. W., *Q. J. Mech. Appl. Math.*, **24** (1971) 263.
[33] Faux D., PhD Thesis, University of Valenciennes, France (2018).
[34] Lehmann F.-O., Sane S. and Dickinson M., *J. Exp. Biol.*, **208** (2005) 3075.